TRANSITION TO TURBULENCE IN PULSATILE STENOTIC FLOWS: A COMBINED EXPERIMENTAL AND NUMERICAL APPROACH

E. Balaras, K. Kiger and B. Parvinian

University of Maryland,
Dept. of Mechanical Engineering,
College Park, MD 20742

INTRODUCTION

Narrowing of a blood vessel, or stenosis, due to substantial plaque deposit, significantly alters the local blood flow dynamics. Over the past several decades, a series of in-vivo and in-vitro studies revealed valuable information on the possible implications of the altered flow dynamics in the pathophysiology of the disease. Early studies that compared measurements in in-vitro models to physiological data showed that plaque thickening appeared in regions of low and oscillatory wall shear stress [1,2]. More recently, additional evidence has emerged explaining the role of hemodynamics and shear stresses on atherosclerosis on a progressively molecular level. Fluid forces have been shown to regulate transcription of growth factors known to regulate smooth muscle cell migration and proliferation [4], as well as transcription by endothelial cells of adhesion molecule genes that attract leukocytes [4].

A number of in-vivo studies [5,6] identified a highly complex flow field in the vicinity of the stenosis, with patches of laminar and disturbed flow regimes that coexist at an instant in time. Although several in-vitro experimental and numerical studies have been performed over the past years, the detailed nature of the flow, especially near the vascular boundary, is still not fully understood. This is due to limitations inherent to the adopted experimental techniques (usually single-point ensemble-averaged information is obtained together with qualitative flow visualizations) or numerical methods (commonly adopted low-order dissipative discretizations and inadequate turbulence models introduce significant inaccuracies).

In the present paper, Direct Numerical Simulations (DNS) will be conducted in simplified models of stenotic vessels under pulsatile flow conditions. A novel non-boundary conforming formulation is adopted to simulate the presence of the stenosis. These simulations will allow for the direct computation of the flow structure near the vascular boundary and its correlation with the wall shear stress, without the need to introduce any add-hoc model. In conjunction with the numerical simulations, scaled experiments are conducted using Particle Image Velocimetry (PIV), which provides instantaneous and cycle-averaged full-field velocity information along the center-plane of the flow. The experimental data provide sufficient detail on the boundary conditions to enable direct comparison with the numerical results. This complementary approach will allow for validation of the adopted numerical method in a prototypical flow, while at the same time giving an increased understanding of the flow physics important to the evolution of post-stenotic transitional flows.

NUMERICAL AND EXPERIMENTAL TECHNIQUES

At this stage of the research, a simplified model of arterial stenosis is considered. A schematic of the geometry and experimental set-up is shown in Figure 1. The test section of the tunnel consists of a $1.3 \times 15.6 \times 180$ cm ($h \times w \times l$) acrylic channel, with a cylindrical segment 50% stenosis placed 35 channel heights upstream of the exit. The flow is provided by a constant head tank, with the pulsatile amplitude controlled using a programmable spool valve and bypass plumbing back to the exit tank. The current configuration is capable of running up to mean Reynolds numbers of 1500 (based on the mean velocity and channel height) with amplitudes of 100%, and can sustain oscillation frequencies, up to 2 Hz. Water is used as the working fluid, giving Wormseley numbers up to 15.

Despite the simplicity of the adopted geometrical configuration described above, conducting DNS for this problem is a challenge for any numerical method available today. In the present study a highly efficient Cartesian solver is used, and the effect of the stenosis is introduced using an ``immersed boundary'' formulation. This approach allows the use of codes in Cartesian coordinates, which present significant advantages in terms of speed, accuracy and flexibility, over codes that employ body fitted grids. In our implementation, the enforcement of non-slip boundary conditions on the vascular boundary is done using a variance of the ``discrete forcing'' approach [7,8]. In [8], the solution is locally reconstructed at the grid nodes in the vicinity of the boundary based on the target boundary conditions, using a simple one-dimensional reconstruction scheme. In the present study we employ a multidimensional procedure proposed by Balaras

[9], where the solution is reconstructed along the well-defined line normal to the interface.

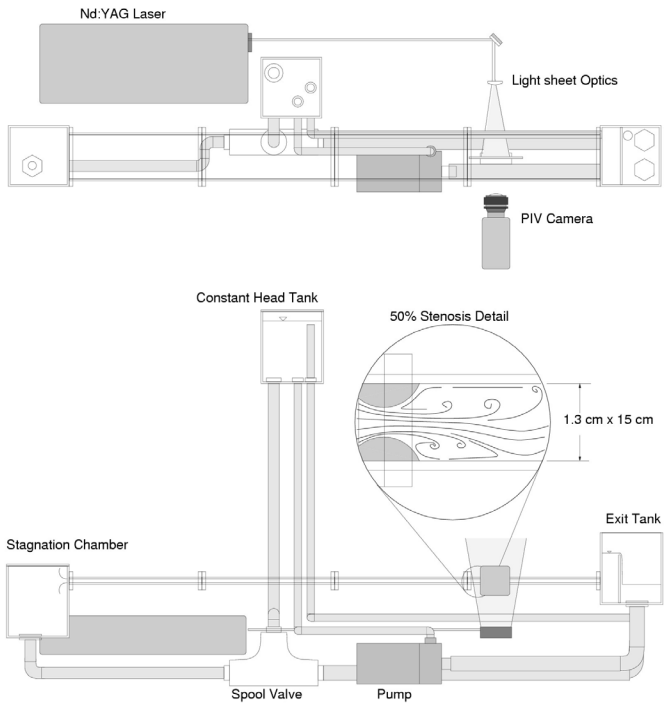

Figure 1: Schematic of the experimental set-up.

The fluid equations are solved using a second order projection method. Both convective and diffusive terms are advanced in time with an explicit Adams Bashforth scheme. The resulting Poisson equation is solved using direct solvers based on Fast Fourier Transforms, or iterative solvers optimized for parallel computations. All spatial derivatives are approximated with second order central differences on a staggered grid. Details on the methodology and implementation in a DNS and LES framework can be found in [9].

Preliminary results for the case of 50% constriction are shown in Figure 2. In this computation, the mean Reynolds number is 1100 and the Wormseley number is 9. The number of grid points is 5.2×10^6. In Figure 2b, isolines of the phase-averaged streamwise velocity are shown at an instant in time just after the peak acceleration. The formation of the jet and the large recirculating areas downstream of the stenosis are evident. In Figure 2b and instantaneous picture of the flow is given at the same instant during the cycle. Isosurfaces of the second invariant of the strain-rate tensor which identify large vortical structures are shown. The presence of the large vortical structures associated with the jet instability can be seen. Further downstream the interaction of the jet with the laminar boundary layer near the vascular boundary couces the later to transition, as it is evident from the packet of hairpin vortices that is generated.

In the full paper the dependence of the above mechanism on the degree of stenosis, Reynolds and Wormseley numbers will be given. Detailed comparisons between simulations and experiments will also be shown.

REFERENCES

1. Friedman, M.H., Hutchins, G.M., Bargeron, C.B., Deters, O.J. and Mark, F.F. 1981, "Correlation of human arterial morphology with hemodynamic measurements in arterial casts," ASME J. Biomech. Eng., 103:204-207.
2. Ku, D.N., Giddens, D.P., Zarins, C.K. and Glagov, S., 1985, "Pulsatile flow and atherosclerosis in the human carotid bifurcation," Atherosclerosis, 5(3):293-302.
3. Mitsumata, M., Fishel, R.S., Nerem, R.M., Alexander, R.W. and Berk, B.C., 1993, "Fluid shear stress stimulates platelet-derived growth factor expression in endothelial cells," Am. J. Physiol. 265:H3-8.
4. Nagel, T., Resnick, N., Atkinson W.J., Dewey, C.F. and Gimbrone, M.A., 1994, "Shear stress selectively upgregulates intercellular adhesion molecule-1 expression in cultured human vascular endothelial cells," J. Clin. Invest., 94:885-891.
5. Stein, P.D and Sabbah, H.N., 1976, "Turbulent flow in the ascending aorta of humans with normal and diseased aortic valves," Circulation Res., 39:58-.
6. Giddens, D.P., Mabon, R.F. and Cassanova, R.A., 1976, "Measurements of disordered flows distal to subtotal vascular stenoses in the thoracic aortas of dogs," Circulation Res., 39:112-
7. Mohd-Yusof, J., 1997, "Combined Immersed Boundaries/B-Splines Methods for Simulations of Flows in Complex Geometries," CTR Annual Research Briefs, NASA Ames/Stanford University.
8. Fadlun, E. A., Verzicco, R., Orlandi, P., and Mohd-Yusof, J. 2000, "Combined Immersed-Boundary Finite-Difference Methods for Three-Dimensional Complex Flow Simulations," J. Comput. Physics, 161:35-60.
9. E. Balaras, 2002, "Modeling complex boundaries using an external force field on fixed Cartesian grids in large-eddy simulations," Computers and Fluids, Submitted for publication.

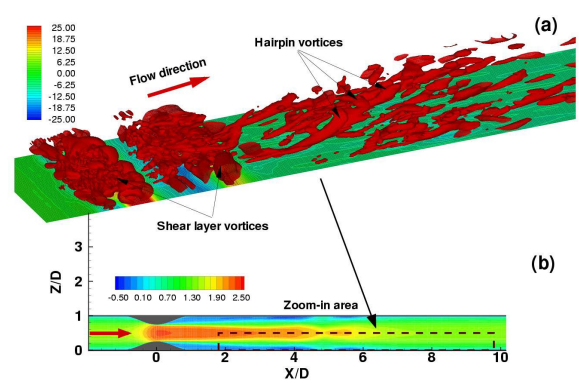

Figure 2: The flow field in the beginning of the deceleration phase. (a) Isosurfaces of the second invariant of the strain-rate tensor at an instant in time; (b) Phase averaged streamwise velocity.